Gaussian Process Latent Force Models for Virtual Sensing in a Monopile-Based Offshore Wind Turbine

Zou, Joanna; Cicirello, Alice; Iliopoulos, Alexandros; Lourens, Eliz Mari

Citation (APA)
Zou, J., Cicirello, A., Iliopoulos, A., & Lourens, E. M. (2022). Gaussian Process Latent Force Models for Virtual Sensing in a Monopile-Based Offshore Wind Turbine. In P. Rizzo, & A. Milazzo (Eds.), *European Workshop on Structural Health Monitoring, EWSHM 2022, Volume 1* (pp. 290-298). (Lecture Notes in Civil Engineering; Vol. 253 LNCE). Springer. https://doi.org/10.1007/978-3-031-07254-3_29

Important note
To cite this publication, please use the final published version (if applicable).
Please check the document version above.

Gaussian process latent force models for virtual sensing in a monopile-based offshore wind turbine

Joanna Zou[1][0000-0003-4457-6186] and Alice Cicirello[1][0000-0002-6556-2149] and Alexandros Iliopoulos[2][0000-0002-5055-4824] and Eliz-Mari Lourens[1][0000-0002-7961-3672]

[1] Delft Institute of Technology, 2628 CD Delft, The Netherlands
[2] Siemens-Gamesa Renewable Energy, 2595 BN The Hague, The Netherlands
j.zou@tudelft.nl

Abstract. Fatigue assessment in offshore wind turbine support structures requires the monitoring of strains below the mudline, where the highest bending moments occur. However, direct measurement of these strains is generally impractical. This paper presents the validation of a virtual sensing technique based on the Gaussian process latent force model for dynamic strain monitoring. The dataset, taken from an operating near-shore turbine in the Westermeerwind Park in the Netherlands, provides a unique opportunity for validation of strain estimates at locations below the mudline using strain gauges embedded within the monopile foundation.

Keywords: Offshore wind turbines, virtual sensing, Bayesian inference, Gaussian process.

Introduction

Fatigue assessment of offshore wind turbines (OWT) is necessary for evaluating the remaining useful life of existing offshore wind farms and validating the design modifications of larger turbines with greater power generation capacity. The support structures of OWT are highly susceptible to fatigue damage, particularly at points below the mudline, due to cyclic wind and wave loading as well as potential resonance effects between the tower's structural frequencies and the turbine's rotor frequencies. In the absence of direct strain measurements, *virtual sensing* provides a means to extrapolate the dynamic response at unmeasured locations using a limited set of vibration measurements at accessible locations of the structure. Various inverse techniques have been proposed for virtual sensing, including a modal decomposition and expansion method which relies on a well-calibrated finite element model and corresponding mode shapes to extrapolate response [1]. However, this approach does not consider the load history to evaluate the influence of environmental and operating conditions. Other techniques use Kalman filtering for stochastic joint input-state estimation [2-3], where the time evolution of the loads ("input") is concurrently predicted with that of the strains ("states"). However, many of these methods idealize

the input as a white noise process, an assumption which may not hold in real-life applications. Moreover, their accuracy depends on prior tuning of covariance matrices for the input and stochastic noise, which is generally conducted by a trial-and-error process, raising questions as to their robustness.

This work proposes to use the *Gaussian process latent force model* (GPLFM) [4,5] for the continuous monitoring of strain time histories below the mudline of an operating OWT. Unlike other Kalman filtering methods, this approach models the input as a Gaussian process driven by a chosen covariance function, offering flexibility in incorporating prior information on its time-varying behavior [4,5]. The GPLFM has been demonstrated to improve upon other joint input-state estimators in numerical studies [4]. This study evaluates the performance of the GPLFM by using vibration data from an operating wind turbine in the Netherlands. The results are validated using strain data recorded along the depth of the monopile foundation.

1   Mathematical Formulation

The goal of joint input-state estimation is to reconstruct the time series of unknown inputs and dynamic response – together, referred to as the "latent states" – when provided with a limited set of acceleration measurements. An abbreviated discussion of the GPLFM methodology is provided; for more details, the reader is referred to [4-7].

1.1   System model

Let the mechanical model of the structural system be represented by the following modally reduced-order model, in which only a subset of dominant modes is retained to represent the dynamics of the system:

$$\tilde{\mathbf{M}}\ddot{\mathbf{r}}(t) + \tilde{\mathbf{C}}\dot{\mathbf{r}}(t) + \tilde{\mathbf{K}}\mathbf{r}(t) = \mathbf{f}(t) \tag{1}$$

$\mathbf{r}(t) \in \mathbb{R}^{n_\mathrm{m}}$ is the modal state vector for a system truncated to n_m modes, related to the original displacement states $\mathbf{u}(t) \in \mathbb{R}^{n_\mathrm{u}}$ by $\mathbf{r}(t) = \mathbf{\Phi}^\mathrm{T}\mathbf{u}(t)$, where $\mathbf{\Phi} \in \mathbb{R}^{n_\mathrm{u} \times n_\mathrm{m}}$ is the matrix of n_m mass-normalized mode shapes. Modal forces are given as $\mathbf{f}(t) = \left[f_1(\mathrm{t})^\mathrm{T} \cdots f_{n_\mathrm{m}}(t)^\mathrm{T}\right]^\mathrm{T} = \mathbf{\Phi}^\mathrm{T}\mathbf{S_p}\mathbf{p}(t)$, where the excitation $\mathbf{p}(t) \in \mathbb{R}^{n_\mathrm{p}}$ acting at the degrees of freedom indicated by $\mathbf{S_p} \in \mathbb{R}^{n_\mathrm{u} \times n_\mathrm{p}}$ are cast into modal coordinates by $\mathbf{\Phi}$. The generalized system matrices are defined as follows: $\tilde{\mathbf{M}} = \mathbf{\Phi}^\mathrm{T}\mathbf{M}\mathbf{\Phi} = \mathbf{I} \in \mathbb{R}^{n_\mathrm{m} \times n_\mathrm{m}}$, $\tilde{\mathbf{C}} = \mathbf{\Phi}^\mathrm{T}\mathbf{C}\mathbf{\Phi} = \mathbf{\Gamma} \in \mathbb{R}^{n_\mathrm{m} \times n_\mathrm{m}} = diag\left(2\xi_j\omega_j^2\right)$, $\tilde{\mathbf{K}} = \mathbf{\Phi}^\mathrm{T}\mathbf{K}\mathbf{\Phi} = \mathbf{\Omega}^2 \in \mathbb{R}^{n_\mathrm{m} \times n_\mathrm{m}} = diag\left(\omega_j^2\right)$, where ξ_j and ω_j are the damping ratio and natural frequency of the jth mode.

Defining the modal state vector $\mathbf{x}(t) = [\mathbf{r}(t)^\mathrm{T} \ \dot{\mathbf{r}}(t)^\mathrm{T}]^\mathrm{T}$, the continuous-time state-space forms of Equation 1 and the measurement model are given as:

$$\dot{\mathbf{x}}(t) = \mathbf{A}_\mathrm{c}\mathbf{x}(t) + \mathbf{B}_\mathrm{c}\mathbf{f}(t) \tag{2}$$
$$\mathbf{y}(t) = \mathbf{G}_\mathrm{c}\mathbf{x}(t) + \mathbf{J}_\mathrm{c}\mathbf{f}(t) \tag{3}$$

$$\mathbf{A}_c = \begin{bmatrix} \mathbf{0} & \mathbf{I} \\ -\mathbf{\Omega}^2 & -\mathbf{\Gamma} \end{bmatrix}, \quad \mathbf{B}_c = \begin{bmatrix} \mathbf{0} \\ \mathbf{I} \end{bmatrix}, \quad \mathbf{G}_c = [-\mathbf{S}_a\mathbf{\Phi}\mathbf{\Omega}^2 \quad -\mathbf{S}_a\mathbf{\Phi}\mathbf{\Gamma}], \quad \mathbf{J}_c = [\mathbf{S}_a\mathbf{\Phi}] \qquad (4)$$

where the selection matrix $\mathbf{S}_a \in \mathbb{R}^{n_y \times n_u}$ indicates the degrees of freedom where acceleration measurements are available, e. g. $\mathbf{y}(t) = \mathbf{S}_a\ddot{\mathbf{u}}(t)$.

1.2 Input model

In the Gaussian process latent force model, each jth modal force is assumed to take the form of a temporal Gaussian process (GP) defined by a mean function and covariance function: $f_j(t) \sim GP\left(\mu_j(t), \kappa_j(t, t'; \boldsymbol{\theta})\right)$ [4,5]. The covariance function $\kappa_j(t, t'; \boldsymbol{\theta})$ is chosen a priori based on knowledge of the time-varying behavior of the input (i. e. periodicity, discontinuity), with properties determined by a set of hyperparameters $\boldsymbol{\theta}$. In the following work, the formulation of a state-space model for a GP with a Matérn covariance function using the smoothing parameter $\nu = 5/2$ is presented; for the generic formulation, the reader is referred to [4,5].

A GP $f_j(t)$ with the Matérn $\nu = 5/2$ covariance function in Equation 5 can be expressed as a realization of the 3rd-order linear time-invariant stochastic differential equation given by Equation 6:

$$\kappa_j(\tau; \alpha, l_s) = \alpha^2 \left(1 + \frac{\sqrt{5}\tau}{l_s} + \frac{5\tau^2}{3l_s^2}\right) \exp\left(-\frac{\sqrt{5}\tau}{l_s}\right) \qquad (5)$$

$$\frac{d^3 f_j(t)}{dt^3} + 3\lambda \frac{d^2 f_j(t)}{dt^2} + 3\lambda^2 \frac{df_j(t)}{dt} + \lambda^3 f_j(t) = w(t) \qquad (6)$$

where $\tau = t - t'$, hyperparameters $\boldsymbol{\theta} = [\alpha, l_s]$, $\lambda = \sqrt{5}/l_s$, and $w(t)$ is a white noise process with spectral density $S_w(\omega) = \sigma_w$. Equation 6 can be reformulated in state-space by constructing the vector $\mathbf{z}_j(t) = \left[f_j(t) \quad \frac{df_j(t)}{dt} \quad \frac{d^2 f_j(t)}{dt^2}\right]^{\mathrm{T}}$:

$$\dot{\mathbf{z}}_j(t) = \mathbf{F}_{c,j}\mathbf{z}_j(t) + \mathbf{L}_{c,j}w(t) \qquad (7)$$

$$f_j(t) = \mathbf{H}_{c,j}\mathbf{z}_j(t) \qquad (8)$$

$$\mathbf{F}_{c,j} = \begin{bmatrix} 0 & 1 & 0 \\ 0 & 0 & 1 \\ -\lambda^3 & -3\lambda^2 & -3\lambda \end{bmatrix}, \quad \mathbf{L}_{c,j} = \begin{bmatrix} 0 \\ 0 \\ 1 \end{bmatrix}, \quad \mathbf{H}_{c,j} = [1 \quad 0 \quad 0] \qquad (9)$$

Because the covariance function is stationary, its Fourier transform is related to the spectral density of the process $f_j(t)$: $\mathcal{F}[\kappa_j(\tau)] = S_{f_j}(\omega)$. The Matérn covariance function belongs to a class of kernels which produce a rational form for $S_{f_j}(\omega)$, such that it can be spectrally factorized as $S_{f_j}(\omega) = H(i\omega)\sigma_w H(i\omega)$, where $H(i\omega)$ is the stable rational transfer function. The spectral density of $w(t)$ is then $\sigma_w = \frac{400\sqrt{5}\alpha^2}{3l^5}$.

In the reduced-order formulation, n_m modal forces are represented by the following block-diagonal state-space system, where $\mathbf{z}(t) = \left[\mathbf{z}_1(t)^\mathrm{T} \cdots \mathbf{z}_{n_\mathrm{m}}(t)^\mathrm{T}\right]^\mathrm{T}$. This study assumes the modal forces are characterized by the same covariance function controlled by a single set of hyperparameters $\boldsymbol{\theta} = [\alpha, l_s]$; $\kappa_1(\tau) = \cdots = \kappa_{n_\mathrm{m}}(\tau) = \kappa(\tau)$.

$$\dot{\mathbf{z}}(t) = \mathbf{F}_\mathrm{c}\mathbf{z}(t) + \mathbf{L}_\mathrm{c}w(t) \tag{10}$$

$$\mathbf{f}(t) = \mathbf{H}_\mathrm{c}\mathbf{z}(t) \tag{11}$$

$$\mathbf{F}_\mathrm{c} = \begin{bmatrix} \mathbf{F}_{\mathrm{c},1} & \cdots & 0 \\ \vdots & \ddots & \cdots \\ 0 & \cdots & \mathbf{F}_{\mathrm{c},n_\mathrm{m}} \end{bmatrix}, \; \mathbf{L}_\mathrm{c} = \begin{bmatrix} \mathbf{L}_{\mathrm{c},1} & \cdots & 0 \\ \vdots & \ddots & \cdots \\ 0 & \cdots & \mathbf{L}_{\mathrm{c},n_\mathrm{m}} \end{bmatrix}, \; \mathbf{H}_\mathrm{c} = \begin{bmatrix} \mathbf{H}_{\mathrm{c},1} & \cdots & 0 \\ \vdots & \ddots & \cdots \\ 0 & \cdots & \mathbf{H}_{\mathrm{c},n_\mathrm{m}} \end{bmatrix} \tag{12}$$

The covariance function of the GP encodes prior information on the variability of $\mathbf{z}(t)$. In this case, $\mathbf{z}(t)$ is a steady-state process because $\kappa(\tau)$ is stationary. For $\mathbf{z}(t) \sim N\big(\mathbf{0}, \mathbf{P}(t)\big)$, the steady-state covariance matrix $\mathbf{P}_\infty$ is the solution to the Lyapunov equation enforcing the steady-state assumption $\mathbf{P}(t) \to \mathbf{P}_\infty, \dot{\mathbf{P}}(t) \to 0$:

$$\dot{\mathbf{P}}(t) = \mathbf{F}_\mathrm{c}\mathbf{P}(t) + \mathbf{P}(t)\mathbf{F}_\mathrm{c}^\mathrm{T} + \mathbf{Q}_\mathrm{c} = \mathbf{F}_\mathrm{c}\mathbf{P}_\infty + \mathbf{P}_\infty\mathbf{F}_\mathrm{c}^\mathrm{T} + \mathbf{Q}_\mathrm{c} = 0 \tag{13}$$

where $\mathbf{Q}_\mathrm{c}$ is the spectral density of the process noise term $\mathbf{L}_\mathrm{c}w(t)$, $\mathbf{Q}_\mathrm{c} = \mathbf{L}_\mathrm{c}\sigma_w\mathbf{L}_\mathrm{c}^\mathrm{T}$. From this expression, it is clear that the hyperparameters $\boldsymbol{\theta}$ chosen to construct the system matrices in Equation 12 define the prior joint distribution assumed for the states $\mathbf{z}(t)$. Optimal values for the hyperparameters are solved for by fitting the covariance observed in the measurement data, typically by maximum likelihood estimation [5,7].

1.3 Latent force model

The latent force model is assembled from the continuous state-space equations of the mechanical system model and stochastic input model. Defining the augmented vector of latent states $\mathbf{z}^a(t) = [\mathbf{x}(t)^\mathrm{T} \; \mathbf{z}(t)^\mathrm{T}]^\mathrm{T}$, the GPLFM is given as:

$$\dot{\mathbf{z}}^a(t) = \mathbf{F}_\mathrm{c}^a\mathbf{z}^a(t) + \mathbf{w}_\mathrm{c}^a(t) \tag{14}$$

$$\mathbf{y}(t) = \mathbf{H}_\mathrm{c}^a\mathbf{z}^a(t) \tag{15}$$

$$\mathbf{F}_\mathrm{c}^a = \begin{bmatrix} \mathbf{A}_\mathrm{c} & \mathbf{B}_\mathrm{c}\mathbf{H}_\mathrm{c} \\ \mathbf{0} & \mathbf{F}_\mathrm{c} \end{bmatrix}, \; \mathbf{w}_\mathrm{c}^a(t) = \begin{bmatrix} \mathbf{0} \\ \mathbf{L}_\mathrm{c}w(t) \end{bmatrix}, \; \mathbf{H}_\mathrm{c}^a = [\mathbf{G}_\mathrm{c} \quad \mathbf{J}_\mathrm{c}\mathbf{H}_\mathrm{c}], \; \mathbf{Q}_\mathrm{c}^a = \begin{bmatrix} \mathbf{0} & \mathbf{0} \\ \mathbf{0} & \mathbf{Q}_\mathrm{c} \end{bmatrix} \tag{16}$$

where $\mathbf{Q}_\mathrm{c}^a$ is the spectral density of the continuous-time process noise $\mathbf{w}_\mathrm{c}^a(t)$. By converting the continuous-time state-space model in Equations 14-16 to discrete-time, the joint posterior inference of latent states is performed recursively using Kalman filtering/RTS smoothing [5]. This methodology is equivalent to performing Gaussian process regression of the acceleration data $\mathbf{y}(t)$, where the time evolution of the latent states is reconstructed through their joint distribution with acceleration states defined in the augmented model. The discrete-time matrices are computed as $\mathbf{F}_\mathrm{d}^a = exp(\mathbf{F}_\mathrm{c}^a\Delta t)$, $\mathbf{H}_\mathrm{d}^a = \mathbf{H}_\mathrm{c}^a$. Whereas the covariance $\mathbf{Q}_\mathrm{d}^a$ of the discrete form of $\mathbf{w}_\mathrm{c}^a(t)$ can be solved for

by matrix fraction decomposition of an integral of $\mathbf{Q}_c^a$ (details in [7]). An alternative is to solve for the steady-state covariance $\mathbf{P}_\infty^a$ from the continuous-time Lyapunov equation in the augmented case (Equation 17), then for $\mathbf{Q}_d^a$ by enforcing the steady-state assumption in the Kalman filter prediction equation (Equation 18). By analogy to Equation 13, the assumed characteristics of the input inherently define its joint distribution with response states, allowing for a fully stochastic representation of the system's dynamic response.

$$0 = \mathbf{F}_c^a \mathbf{P}_\infty^a + \mathbf{P}_\infty^a (\mathbf{F}_c^a)^T + \mathbf{Q}_c^a \tag{17}$$

$$\mathbf{P}_\infty^a = \mathbf{F}_d^a \mathbf{P}_\infty^a (\mathbf{F}_d^a)^T + \mathbf{Q}_d^a \tag{18}$$

2 In-Situ Validation

2.1 Measurement setup and data processing

The dataset used in this study is taken from the W27 turbine, located in the near-shore Westermeerwind wind farm in the IJsselmeer Lake of the Netherlands. The dataset consists of (a) SCADA data collected from the rotor-nacelle assembly (RNA) at 95.0m above the mean water level (NAP), which includes wind speed, rotor speed, nacelle yaw angle, and acceleration in the fore-aft (FA) and side-side (SS) directions of the turbine; (b) acceleration data, from one accelerometer measuring along the 39.4-219.4 line (from North) at +42.5m NAP and two orthogonally positioned accelerometers at +4.5m NAP, measuring in the North-South and East-West directions respectively; and (c) vertical strain data, from a total of eight rings each containing four strain gauges, labeled A-D. Six of the rings are embedded in the pile below the mudline, concentrated in the region where the highest bending moments are expected to occur, and two rings
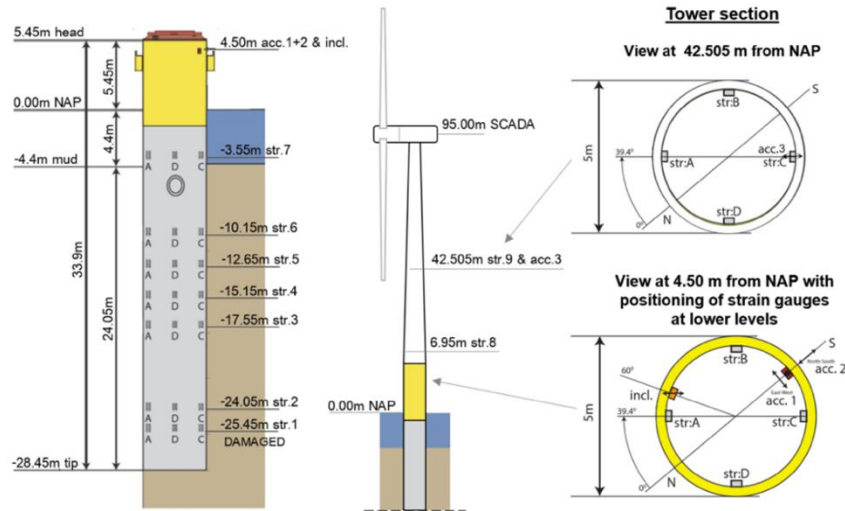

Fig. 1. Position of strain gauges, accelerometers, and SCADA system, from [8].

are located on the support structure above NAP. The layout and orientation of the sensors are illustrated in Figure 1. Ring 1 is not included because the strain gauges were damaged during pile installation.

The data is recorded continuously in 10-minute periods and synchronized to a sampling frequency of 50 Hz. Since only dynamic strains are considered in this work, the data is detrended to be zero-mean and processed with a bandpass Chebyshev Type II filter with stopband frequencies of 0.15 Hz and 5.0 Hz.

2.2 System model

To develop a system model of the support structure, a finite element (FE) model is constructed based on known geometric and material properties of the W27 turbine. The FE model consists of 100 Timoshenko beam elements with pipe cross sections, with variable diameters to represent the tapered profile of the tower. The monopile and tower are made of structural steel with E=210 GPa, v=0.3, and mass density of 7850 kg/m^3. External components such as the RNA, platform, and power unit are modeled as concentrated masses. To model the soil foundation, first a mass density of 1500 kg/m^3 representing the soil plug is added to the elements located below the mudline [8]. Then, a stiffness profile derived from [8] is added to the lateral stiffness of the elements below the mudline. The stiffness profile is a high-fidelity model of the soil-structure system, as it is developed from dynamic experiments conducted at the site of the W27 turbine prior to installation of the support structure.

The FE model is then updated to match the modal parameters of the structure identified by the SSI-Cov [9,10] operational modal analysis (OMA) method. The data samples used for OMA are carefully selected based on the sensor setup to allow for accurate identification of the FA and SS modes. Because accelerometer 3 at +42.50m NAP is uniaxial and cannot provide full measurements of two-dimensional motion, the samples chosen are ones where the OWT is oriented such that the RNA aligns with the axis of accelerometer 3 and the measurement corresponds directly to the FA or SS motion. Only samples where the OWT is idling are used for OMA, as the ambient loading in this condition most closely matches the assumption of white noise input in the SSI-Cov method [9]. A comparison of the mode shapes identified by OMA and those corresponding to the final FE model is illustrated in Figure 2. Table I shows good agreement between the measured and computed modal parameters for the first five modes of the OWT.

Table 1. Error statistics on modal properties.

No.	Mode	f_{id} (Hz)	f_{fem} (Hz)	ξ_{id} (%)	MAC
1	1st FA bending	0.296	0.296	1.932	0.999
2	1st SS bending	0.290	0.296	3.011	0.995
3	2nd FA bending	1.869	1.873	2.379	0.999
4	2nd SS bending	1.885	1.873	2.887	0.927
5	3rd SS bending	4.563	5.207	2.604	0.870
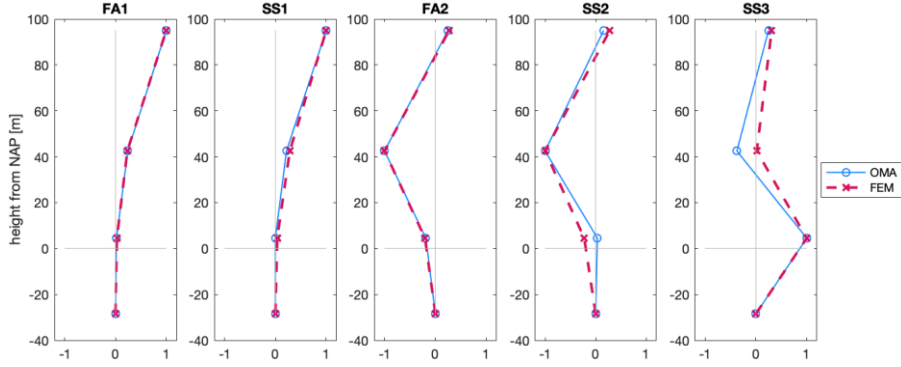
Fig. 2. First five displacement mode shapes, identified by OMA (solid blue) and fitted with FEM (dashed red).

2.3 Results

The performance of the GPLFM is validated with data in the FA direction of the OWT in its power production state, with an ambient wind speed of 22 m/s.

As discussed earlier, the fit of the latent force model depends on (a) the covariance function and its corresponding hyperparameters used to represent the unknown input, which governs the prior belief placed on all augmented states; and (b) the accuracy of the FE model in capturing the mode shapes of the system. The predicted acceleration response is compared with the measurements in Figure 3 as a "diagnostic tool" for checking the fit of the model. In the left-most column of Figure 3, the dashed black lines indicate the empirical variance of each acceleration channel, shown as confidence bounds of ±3 standard deviations, computed directly from the measurement history. The dashed red lines indicate the prior variance placed on acceleration states based on the stochastic augmented model, where the covariance matrix is computed as $\widehat{\mathbf{P}}_0^{\ddot{u}} = \mathbf{H}_c^a \mathbf{P}_\infty^a (\mathbf{H}_c^a)^\mathrm{T}$. The excellent match in variances indicates that the properties assumed for input are an appropriate fit to the data. This result is apparent in the strong match between the measured and predicted acceleration time series, with a mean correlation coefficient of 0.974 and mean relative error of 2.3% across the three channels. In the frequency domain, there are small discrepancies observed at the level of accelerometer 1-2 and 3. The error occurs at frequencies across the PSD which are less excited relative to the first and second modal frequencies of the system (at 0.296 Hz and 1.869 Hz, respectively), which consistently dominate the response over time.

Figure 4 shows that the strain response is overestimated in the time domain. This discrepancy is reflected by a higher mean relative error of 6.0% across all eight strain gauge channels. Difficulties in estimating the strain magnitude are associated with uncertainty in the modeled soil stiffness, particularly at lower depths along the monopile foundation where greater error is observed. However, a good match in the frequency content is indicated by a high mean correlation coefficient of 0.956. Even though the strain response is dominated by the first mode, higher frequency strain response is estimated well due to the high accuracy in the estimated acceleration response of the system.
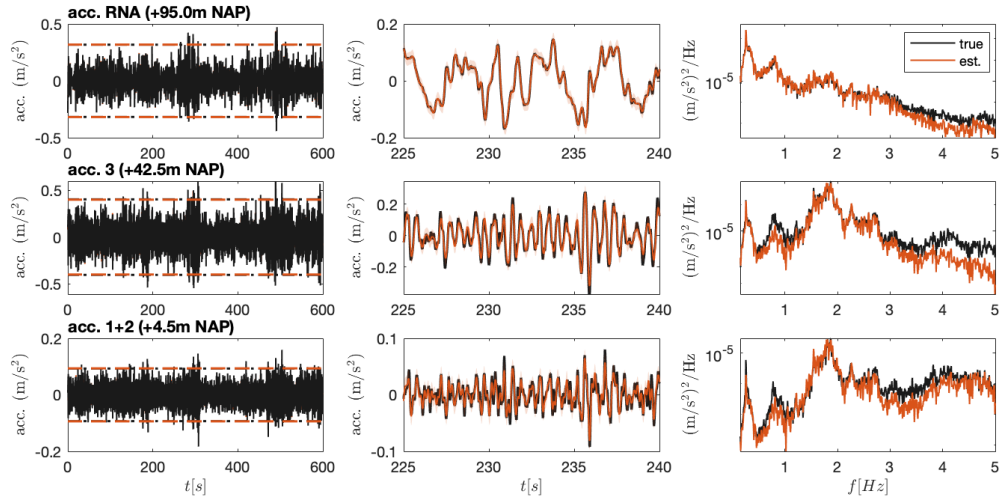
Fig. 3. The 10-minute time series, close-up view of the time series, and frequency spectrum of the true (black) and predicted (red) accelerations for the three sensor channels. $\pm 3\sigma$ confidence bounds on the prediction are shown in shaded red.
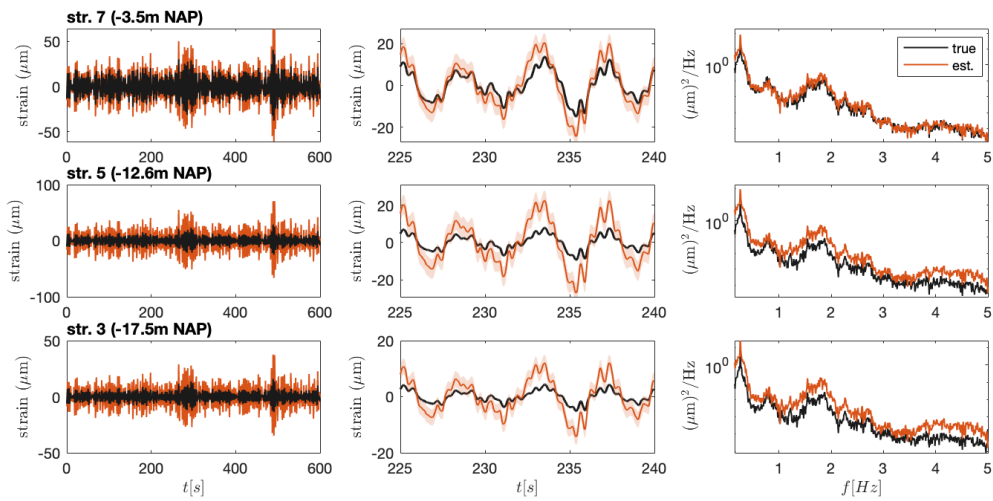
Fig. 4. The 10-minute time series, close-up view of the time series, and frequency spectrum of the true (black) and predicted (red) strains at sensor channels 3, 5, and 7. $\pm 3\sigma$ confidence bounds on the prediction are shown in shaded red.

3   Concluding Remarks

The GPLFM is implemented for virtual sensing of an offshore wind turbine in the Netherlands, where the strain estimation is validated using measurements below the mudline. It is demonstrated that the GPLFM offers a data-driven approach to deriving the covariance of the latent states, leading to high overall accuracy. Strong results for acceleration estimation are presented; however, the method displays an overestimation of the dynamic strain magnitude. In future work, the robustness of the GPLFM will be tested using multiple data samples of the OWT in various operating conditions, as well as its sensitivity to uncertainty in the foundation model.

References

1. Iliopoulos, A., Shirzadeh, R., Weijtjens, W., Guillaume, P., van Hemelrijck, D., Devriendt, C.: "A modal decomposition and expansion approach for prediction of dynamic responses on a monopile offshore wind turbine using a limited number of vibration sensors." *MSSP*, 68-69: 84-104 (2016).
2. Noppe, N., Tatsis, K., Chatzi, E., Devriendt, C., Weijtjens, W.: "Fatigue stress estimation of offshore wind turbine using a Kalman filter in combination with accelerometers." *ISMA 2018* (2018).
3. Tatsis, K., Lourens, E.: "A comparison of two Kalman-type filters for robust extrapolation of offshore wind turbine support structure response." *IALCCE 2016*. (2016).
4. Nayek, R., Chakraborty, S., Narasimhan, S.: "A Gaussian process latent force model for joint input-state estimation in linear structural systems." *MSSP*, 128: 497-530 (2019).
5. Hartikainen, J., Sarkka, S.: "Kalman filtering and smoothing solutions to temporal Gaussian process regression models." *MLSP 2010* (2010).
6. Rogers, T. J., Worden, K., Cross, E. J.: "On the application of Gaussian process latent force models for joint input-state-parameter estimation: With a view to Bayesian operational identification." *MSSP*, 140: 106580 (2020).
7. Sarkka, S.: Recursive Bayesian inference on stochastic differential equations (PhD thesis). Helsinki University of Technology (2006).
8. Versteijlen, W. G., Renting, F. W., van der Valk, P. L. C., Bongers, J., van Dalen, K. N., Metrikine, A. V.: "Effective soil-stiffness validation: Shaker excitation of an in-situ monopile foundation." *Soil Dyn. & Earthquake Eng.,* 102: 241-262 (2017).
9. Peeters, B., de Roeck, G.: "Reference-based stochastic subspace identification for output-only modal analysis." *MSSP*, 13(6): 855-878 (1999).
10. Boroschek, R., Bilbao, J.A.: "Interpretation of stabilization diagrams using density-based clustering algorithm." *Engineering Structures*, 178: 245-257 (2019).
11. Maes, K., De Roeck, G., Iliopoulos, A., Weijtjens, W., Devriendt, C., Lombaert, G.: "Kalman filter based strain estimation for fatigue assessment of an offshore monopile wind turbine." *ISMA 2016* (2016).